Light-induced improvement on performance of $MAPbI_{3-x}Cl_x$ perovskite nanowires solar cells

JIABIN HAO[1,*], ZEMING WANG[2], HONGCHENG GAO[1,*], XIAOXUAN LI[1], BO YANG[1], XU HE[3]
[1]*Department of Chemical Engineering, Hebei Petroleum University of Technology, Chengde 067000, P. R. China*
[2]*Hebei Tourism Vocational College, Chengde 067000, P. R. China*
[3]*514 Brigade of North China Geological Exploration Bureau, Chengde 067000, P. R. China*

One-dimensional perovskite nanowires (PNWs) materials have attracted attention in integrated photonics and photovoltaic device due to their unique optoelectronic properties, such as large-scale optoelectronic integration, high-density data storage and low defect states density. However, many fundamental questions concerning structure and performance, especially the light-induced performance changes in the PNWs solar cells are still unclear. In this work, a continuous light irradiation (0-90 mins) was carried out to study the device performance, structure changes and electrochemical dynamics property in $MAPbI_{3-x}Cl_x$ PNWs devices. We observed that the device efficiency first increases and then decreases with the prolongation of light illumination time. When the illumination reaches to 5 mins, the device exhibits a highest PCE of 15.06%, which possibly due to structural change caused by the ion migration and accumulation. The possible mechanism was elaborated for the first time.

(Received September 30, 2022; accepted June 9, 2023)

Keywords: $MAPbI_{3-x}Cl_x$ PNWs, Solar cells, Light illumination, Ion migration

1. Introduction

Organic-inorganic perovskite, the active layers in solar cells, have exhibited unusual properties such as high optical coefficient, long carrier diffusion length, and tunable band gap [1-4]. Despite the rapid development in power conversion efficiency of perovskite devices as high as 25% [5], many main questions concerning such as current−voltage hysteresis, device instability and structural-electronic properties are still unknown, which have become barriers restricting the improvement of devices efficiency. Several strategies, including defect passivation, element doping, design of chemically inert carbon-based electrodes have been used to improve the performance and stability of the perovskite device [6].

With respect to the bulk structure, PNWs has superior optical properties, more observable spatial optical/electrical properties and lower defect states density, which make them suitable to be used in a broad range of applications [7-12]. Shang et al. introduced metal-insulator-semiconductor (MIS) hybrid plasmonic cavity that enhanced strong exciton–photon interaction in $CH_3NH_3PbBr_3$ perovskite NWs [9]. The PNWs supersede their bulk counterparts with remarkable optoelectronic properties which achieved recently promising performances in perovskite solar cells. Im et al. reported the perovskite NWs solar cell with a best PCE of 14.71% by the two-step spin-coating method for the first time [11]. Wang et al. reported a feasibly room temperature synthesis method was developed for perovskite nanowires [12]. Besides, the excellent photon-to-electron conversion efficiency and the external quantum efficiency of PNWs has been applied in the nanoscale devices [13-15]. Benefiting from the naturally formed end-facets of ZnO NW, Yang and co-workers realized the first optically pumped NW lasing [13]. Zhang and co-workers fabricated vertically integrated MHP quantum wire/nanowire (QW/NW) array based on photodetectors in nanoengineered porous alumina membranes (PAMs) showing self-driven broadband photodetection (BPD) and NPD capability simultaneously [14]. Thus far, light-induced optoelectronic properties study in perovskite NWs solar cells is still lacking.

In this paper, we fabricated $MAPbI_{3-x}Cl_x$ PNWs solar cells and measured the solar cell performances under continuous light irradiation. With increase of illumination time, the PCE of PNWs solar cells increased first and then decreased because of carrier transport and ion-migration-induced structural change in $MAPbI_{3-x}Cl_x$ PNWs solar cells. We further performed light illumination and voltage bias test to investigate the ion migration influences on a lateral structure. Visible ion migration and accumulation phenomenon in PNWs could gradually observed with prolonged illumination. Meanwhile, the evidence obtained from the Steady-state PL spectrum shows suppressed non-radiative recombination in PNWs in the comparison of the bulk perovskite film. Our work provides an insight into light-induced optoelectronic properties variation and related influences in PNWs and devices, which is strongly desired not only for the development of PNWs material but also for the perovskite-based devices.

2. Experimental

2.1. Fabrication of devices

The compact TiO_2 precursor consisting of 100 μL titanium (IV) isopropoxide, 2.5 mL ethanol and 20 μL dilute hydrochloric acid stirred for 20 min was spin-coated on FTO substrates at 3000 rpm for 30s and subsequently sintering at 500 °C for 30 min. The substrates were further treated with 40 mM $TiCl_4$ aqueous solution at 70 °C for 30 min in the oven, and then cleaned with deionized water to sinter at 500 °C for 30 min to obtain the electron transfer layer. To prepare the mesoporous TiO_2 layer, a TiO_2 paste diluted by ethanol of 1:7 weight ratio was spin-coated at 4500 rpm for 40 s and then baked at 500 °C for 30 min. After cooling to room temperature, the TiO_2 films were immersed into 20 mM $TiCl_4$ solution at 70 °C for 30 min and then heated treated at 500 °C for 30 min.

$MAPbI_{3-x}Cl_x$ PNWs was obtained by a modified two-step spin-coating method. 1 M PbI_2 solution in DMF was spin-coated on the mesoporous TiO_2 layer, and then CH_3NH_3I/CH_3NH_3Cl (MAI/MAC) (a molar ratio of 1:1) isopropanol solution with different volumes of DMF (0 μL, 20 μL, 60 μL, 100 μL, 150 μL and 200 μL) was spin-coated on PbI_2 film at 4000 rpm for 20 s. The films were annealed at 110 °C for 10 min to obtain $MAPbI_{3-x}Cl_x$ PNWs materials.

The hole transport layer was prepared by dissolving 72.3 mg spiro-OMeTAD in 1 mL chlorobenzene with additives consisting of 17.5 μL Li-TFSI/acetonitrile (520 mg/mL), 28.8 μL of TBP. The hole transport material was spin-coated at 2000 rpm for 40 s. Ag electrode with 100 nm was deposited on the top of the device using thermal evaporation. Finally, the Ag-doped perovskite solar cells were successfully obtained.

2.2. Characterization techniques

X-ray diffraction (XRD) test were carried out by an X-ray power diffractometer (D8 Ad-vance, Bruckers AXS, Cu Ka radiation). A S-4800 scanning electron microscope (SEM) with energy-dispersive spectroscopy (EDS) was used to observe the morphological properties and test the elements distribution changes, especially iodide ions, in the PNWs films after light illumination. Photocurrent density–voltage (J–V) curves of solar cells were measured with a Keithley 2400 source meter under the simulated AM 1.5G illumination at a calibrated intensity of 100 mW/cm^2 by a Class AAA solar simulator at room temperature in the air. Steady-state photo-luminescence (PL) spectroscopy was measured with an excitation wavelength of 510 nm.

3. Results and discussion

From the SEM images, we see the typical morphology of the perovskite nanocrystals shown in Fig. 1(a). Then PNMs starts to form when dipping MAI/MAC solution with 20 μL DMF presented in Fig. 1(b). The amount of $MAPbI_{3-x}Cl_x$ perovskite NMs gradually increases when increased to 60 μL DMF. Furthermore, the perovskite film exhibits a uniform NMs surface morphology with 100 μL DMF in Fig. 1(d), indicating a larger charge transport influence on devices. Obviously, 1D $MAPbI_{3-x}Cl_x$ PNWs films were prepared by using 150 μL and 200 μL DMF shown in Fig. 1(e) and (f), which could be ascribed to more preferential react sites of PbI_2 and MAI/MAC. Thus, the uniform and dense PNMs layer can lead to a faster carrier separation as well as a higher lateral conductivity.

The morphology of the perovskite thin film has an impact on the photoelectric conversion performance of the device. The sample with 0 μLDMF has a typic perovskite bulk structure. The device delivers a PCE of 10.45%. The PNWs start to form when dipping 20 μL DMF. The device delivers a PCE of 9.86%. The amount of PNMs gradually increases when increased to 60 μL DMF. The device has s a PCE of 11.93%. When the 100 μL DMF was dipped, exhibits a uniform perovskite nanowires surface. Furthermore, the results show the more dense and uniform surface morphology with dipping 150 μL and 200 μL DMF. The devices exbibits the PCE of 12.23%, 12.16% and 11.44%, respectively. The corresponding J-V curves are presented in Fig. 2.

To study the crystal structure in PNWs, the X-Ray diffractograms (XRD) were investigated shown in Fig. 3(a). All samples exhibit the tetragonal $MAPbI_{3-x}Cl_x$ perovskite structure. Compared with the pristine sample, the PbI_2 peak intensity of both PNWs samples prepared by using 100 μL and 150 μL DMF were much lower, indicating a higher crystalline quality, which possibly because a larger amount of PbI_2 was released into MAI/MAC solution in the NWs formation process.

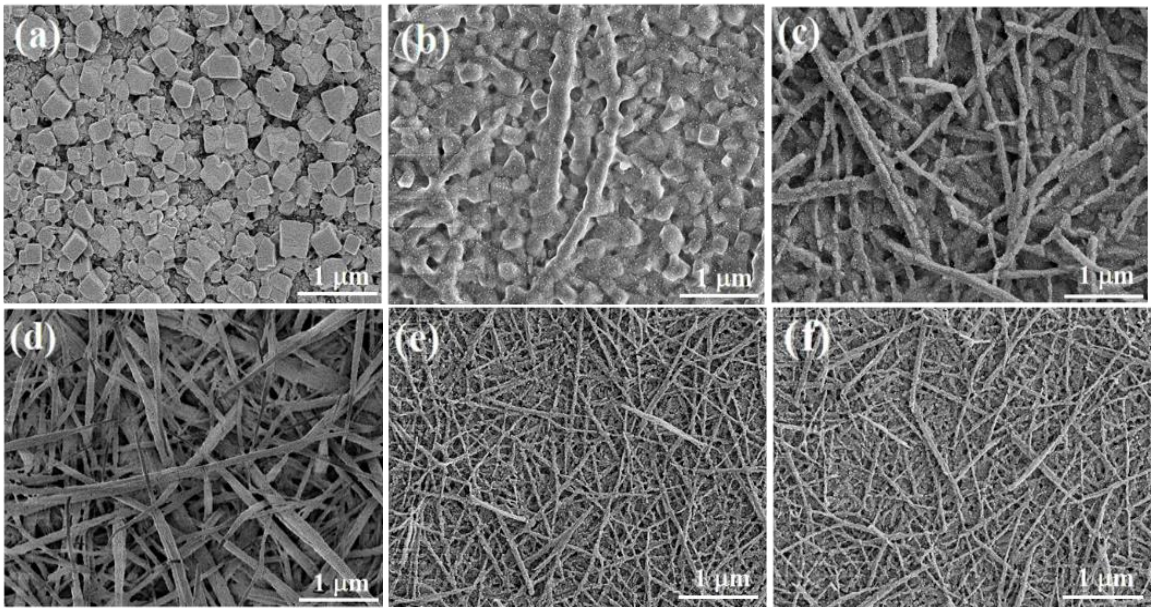

Fig. 1. SEM images of the $MAPbI_{3-x}Cl_x$ PNWs prepared by using DMF solution with (a) 0 μL, (b) 20 μL, (c) 60 μL, (d) 100 μL, (e) 150 μL and (f) 200 μL DMF

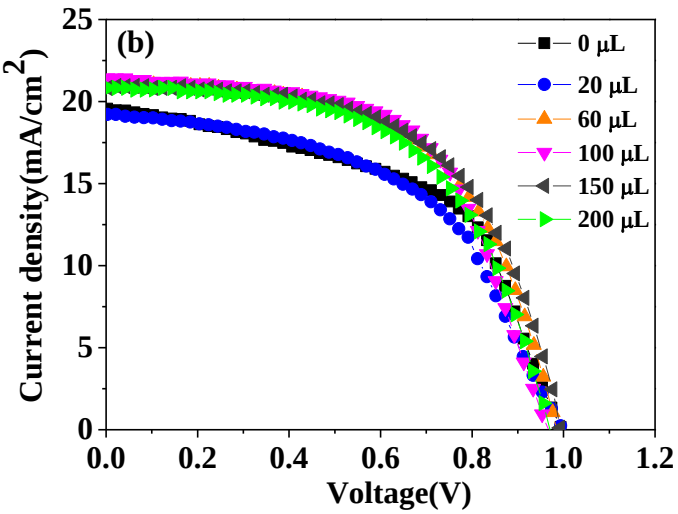

Fig. 2. J-V curves of the $MAPbI_{3-x}Cl_x$ PNWs prepared by using DMF solution with 0 μL, 20 μL, 60 μL, 100 μL, 150 μL and 200 μL

Fig. 3(b) shows the steady-state PL of PNWs layer prepared on TiO_2/FTO films. As evidenced by the PL results, the samples exhibited a decrease of PL intensity, suggesting that the non-radiative carrier recombination losses were suppressed. Therefore, the defect and trap states were reduced in in the PNWs compared to the control 3D perovskite film. In this regard, we speculate that the accumulation of I^- near the positive electrode could induce enhanced PL quantum efficiency, which is consistent with the device performance results.

The photocurrent density-voltage (J-V) curves are presented in Fig. 4. Table 1 shows the device displays an initial efficiency of 13.02%, and then the PCE improved to 13.91% and 14.05% after 1- and 3-mins, respectively. The better performance can be mainly due to the enhanced carrier separation at interface. When the illumination reaches to 5 mins, the device exhibits a highest PCE of 15.06% with a highest V_{oc} of 1.04 V, a highest J_{sc} of 23.31 mA/cm^2 and a highest FF of 0.621. Such an obvious performance enhancement result from the built-in electric field caused by ion migration in PNWs; that is, both I^- and MA^+ ions with activation energies drift to the area near the electrode under light illumination, respectively. The p-type doping band bending caused by accumulation of I^- led to increase of the local photocarrier density. However, the local carrier density varies slightly due to the drift and migration of MA^+ ions caused by the negative polarization, which could be ascribed to reversible structural swell−shrink induced by MA^+ ion migration [13]. After 10 mins, the device performance shows a significant decrease. The PCE dramatically decrease to 7.20% after light-soaking of 90 mins, which occurs possibly because of the decomposition of perovskite materials.

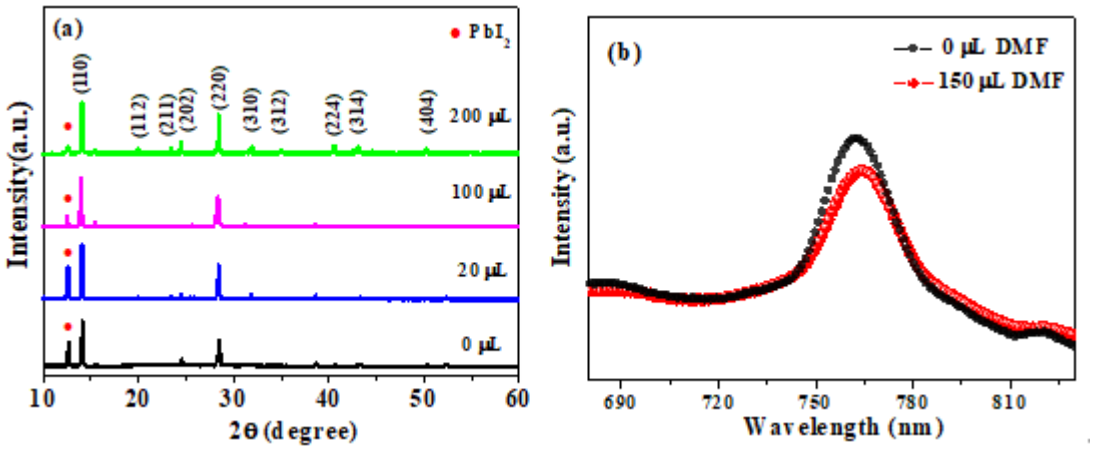

Fig. 3. (a) XRD patterns of $MAPbI_{3-x}Cl_x$ PNWs film prepared by using different amount of DMF; (b) The Steady-state PL of $MAPbI_{3-x}Cl_x$ perovskite layer prepared on TiO_2/FTO films (color online)

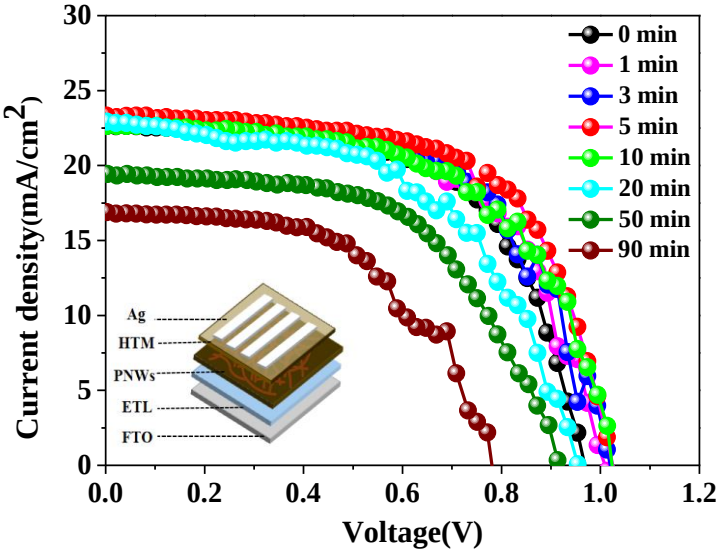

Fig. 4. J-V curves of perovskite NMs device at continuous light irradiation (color online)

Table 1. Photovoltaic performances summary of the perovskite devices

Light time(mins)	Voc (V)	Jsc (mA/cm^2)	FF	PCE (%)
0	1.02	22.83	0.559	13.02
1	1.02	22.84	0.597	13.91
3	1.03	22.85	0.597	14.05
5	1.04	23.31	0.621	15.06
10	1.03	22.64	0.587	13.69
20	0.99	22.93	0.534	12.13
50	0.94	19.84	0.544	10.14
90	0.81	16.89	0.526	7.20

In this work, a constant voltage of 100 V was applied in a latera structure of a $MAPbI_{3-x}Cl_x$ PNWs film between two Ag electrodes to simulate the poling process, which is used to further investigate the changes in structure and photoelectric properties upon ion migration. Fig. 5(a) and (b) was used to simulate the poling electric field change process in PNWs. The morphology of the PNWs and bulk perovskite film under neither light nor bias are shown in

Fig 5(c) and (f), respectively. Obviously, a dark line along the positive electrode edge can be observed under light illumination and bias for 5 mins, which is induced by I^- ion migration and accumulation, as shown in Fig 5(d) [16, 17]. When the light time was 10 mins, the dark line was obviously much wider, as shown in Fig. 5(e) and (h). Notably, the delamination cracks appeared at the edge of the positive electrode, which could be ascribed to a lattice structural expansion caused by prolonged light-soaking irradiation. However, almost no change can be observed in the region near the negative electrode. In comparison to the bulk perovskite material, the above phenomenon in the polarization process is more serious in nanowires, possibly because of the faster ion migration and accumulation in PNWs than that in bulk sample. We concluded that a short light illumination time induced the enhanced built-in electric field caused by ion migration, and then the device performance will be improved. When ex-posed to light for a long time, the decomposition of perovskites will lead to a structural change, resulting in a decreased cell efficiency. We speculated that the performance improvement could be ascribed to the structural change; that is, the accumulation of I^- may result in a light-induced increase of photoelectric conversion process [18, 24].

To investigate the electrochemical dynamics in the perovskite nanowire solar cell, the electrochemical impedance spectroscopy (EIS) of the device with light illumination after 0 and 5 mins, as shown in Fig. 6(a). A relatively equivalent circuit which consists of the series resistance (R_1), the selective contact resistance (R_2), the interface-related resistance (R_3) and two nonideal capacitive element called constant-phase element (CPE_1 and CPE_2) is applied to fit the impedance response, as presented in Fig. 6(b) [19-22]. In general, the resistance coupled with R_2 and CPE_1 is associated with the charge transport condition between contact layers in perovskite nanowire devices, which is in the high and moderate frequency region of the Nyquist plots curve. The resistance, R_3 is coupled with CPE_2 in the low-frequency region and associated with the accumulation resistance, charge recombination at interfaces, and ion diffusion process in devices [23]. Meanwhile, the Warburg diffusion resistance (Wo) related to the ion movement of the whole perovskite nanowire device [19].

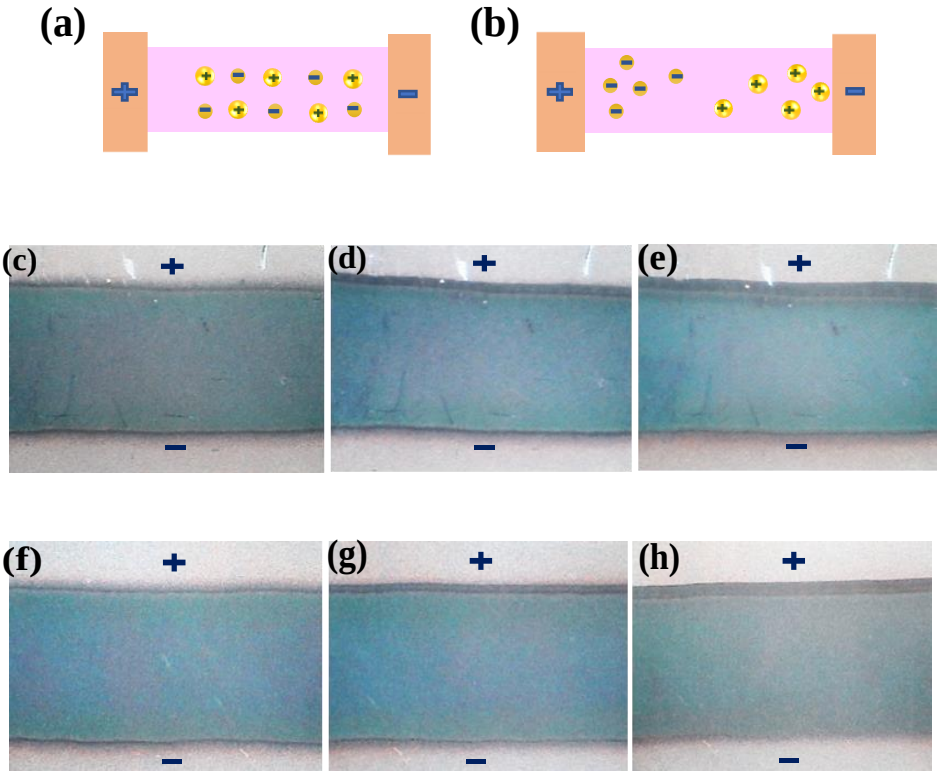

Fig. 5. (a−b) Schematics of ion migration in a PNWs material under poling conditions; Topography maps of (c-e) the MAPbI3-xClx PNWs film and (f-h) the bulk perovskite film with a voltage of 100 V (color online)

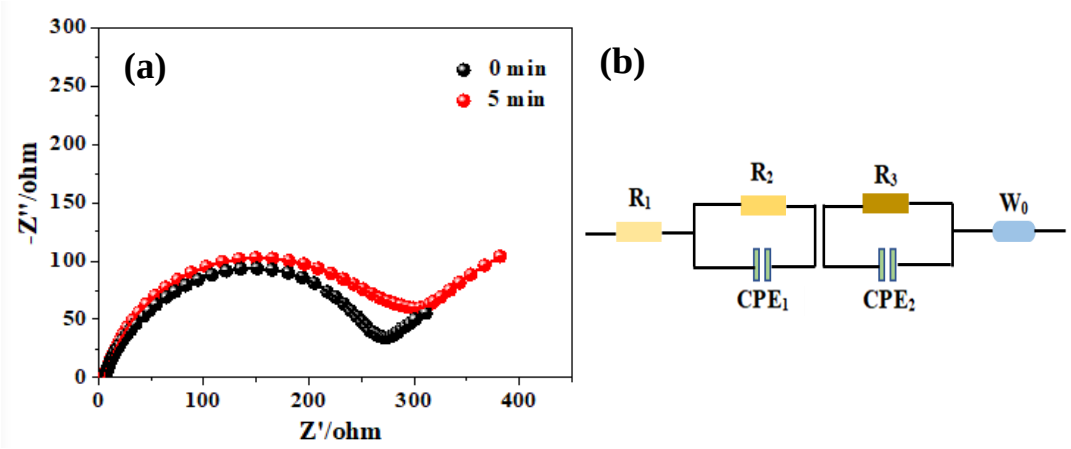

Fig. 6. (a) The electrochemical impedance spectroscopy (EIS) of the device with light illumination after 0 and 5 mins; (b) Equivalent circuit model for the solar cell (color online)

4. Conclusions

In this work, we successfully fabricated $MAPbI_{3-x}Cl_x$ PNWs solar cells by a modified two-step spin-coating method. The influence of continuous light illumination on the de-vice performance was studied. We observed that the photovoltaic performance of PNWs devices continues to increase until it starts to decrease after 5 minutes, and then a best PCE of 15.06% was obtained. Compared to the bulk perovskite, $MAPbI_{3-x}Cl_x$ PNWs materials displayed a suppression of non-radiative recombination in the defects, which is ascribed to high specific surface area and the lateral conductivity of NWs structure. Moreover, a slower charge recombination at interfaces in $MAPbI_{3-x}Cl_x$ PNWs device after 5 mins light illumination. This is because the enhanced built-in electric field caused by light-induced I-migration of ionic species in the perovskite nanowire layer, which is an important influence on improved performance of $MAPbI_{3-x}Cl_x$ PNWs solar cells.

Acknowledgements

This work is supported by Science and Technology Planning Project from Hebei Provincial Department of Education, China (QN2023068, QN2023018).

References

[1] M. K. Nazeeruddin, H. Snaith, MRS Bulletin **40**(8), 641 (2015).
[2] S. D. Stranks, G. E. Eperon, G. Grancini, C. Menelaou, M. J. P. Alcocer, T. Leijtens, L. M. Herz, A. Petrozza, H. J. Snaith, Science **342**(6156), 341 (2013).
[3] D. Gao, L. Yang, X. Ma, X. Shang, C. Wang, M. Li, X. Zhuang, B. Zhang, H. Song, J. Chen, C. Chen, Journal of Energy Chemistry **69**, 659 (2022).
[4] K. Lin, J. Xing, L. N. Quan, F. Pelayo Garcia de Arquer, X. Gong, J. Lu, L. Xie, W. Zhao, D. Zhang, C. Yan, W. Li, X. Liu, Y. Lu, J. Kirman, E. H. Sargent, Q. Xiong, Z. Wei, Nature **562**(7726), 245 (2018).
[5] Z. Zhang, Y. Liu, P. Zhang, Y. Mao, Organic Electronics **88**, 106007 (2021).
[6] G. Yang, Z. Ren, K. Liu, M. Qin, W. Deng, H. Zhang, H. Wang, J. Liang, F. Ye, Q. Liang, H. Lin, Y. Chen, Y. Zhuang, S. Li, B. Gao, J. Wang, T. Shi, X. Wang, X. Lu, H. Wu, J. Hu, D. Lei, S. K. So, Y. Yang, G. Fang, G. Li, Nature Photonics, **15**(9), 681 (2021).
[7] X. Li, Y. Chen, L. Li, J. Huang, Materials **11**, 1759 (2018).
[8] X. Li, L. Li, Z. Ma, J. Huang, F. Ren, Optik **142**, 293 (2018).
[9] Q. Shang, S. Zhang, Z. Liu, J. Chen, P. Yang, C. Li, W. Li. Y. Zhang, Q. Xiong, X. Liu, Q. Nano Letters **18**(6), 3335 (2018).
[10] W. Deng, L. Huang, X. Xu, X. Zhang, X. Jin, S.-T. Lee, J. Jie, Nano Letters **17**(4), 2482 (2017).
[11] J. H. Im, J. S. Luo, M. Fanckevicius, N. Pellet, P. Gao, T. Moehl, S. M. Zakeeruddin, M. K. Nazeeruddin, M. Gratzel, N.-G. Park, Nano Letters **15**, 2120 (2015).
[12] Y. Wang, X. Liu, Q. He, G. Chen, Advanced Functional Materials **31**(22), 2011251 (2021).
[13] Y. Zhang, Y. Wang, Z. Q. Xu, J. Xue, Z. Wang, J. Zheng, L. Jiang, C. Zheng, F. Huang, B. Sun, Y.-B. Cheng, Q. Bao, ACS Nano **10**(7), 7031 (2016).
[14] D. Zhang, Y. Zhu, Q. Zhang, B. Ren, B. Cao, Q. Li, S. Poddar, Y. Zhou, X. Qiu, Z. He, Z. Fan, Nano Letters **22**(7), 3062 (2022).
[15] J. Cha, M. K. Kim, W. Lee, H. Jin, H. Na, D. G. T. Nguyen, S.-H. Lee, J. Lim, M. Kim, Chemical Engineering Journal, **451**, 138920 (2023).
[16] P. Zardari, A. Rostami, Solar Energy Materials and Solar Cells **227**, 111119 (2021).
[17] L. Jiang, J. Lu, S. R. Raga, J. Sun, X. Lin, W. Huang, F. Huang, U. Bach, Y. B. Cheng, Nano Energy **58**, 687 (2019).
[18] V. W. Bergmann, S. A. L. Weber, F. Javier Ramos, M. K. Nazeeruddin, M. Gratzel, D. Li, A. L. Domanski, I. Lieberwirth, S. Ahmad, R. Berger, Nature communications **5**(1), 1 (2014).
[19] A. R. Pascoe, N. W. Duffy, A. D. Scully, F. Huang,

Y.-B. Cheng, Journal of Physical Chemistry C **119**(9), 4444 (2015).
[20] C. Fei, L. Guo, B. Li, R. Zhang, Nano Energy **27**, 17 (2016).
[21] I. Zarazua, S. Sidhik, T. Lopez-Luke, D. Esparza, E. de la Rosa, J. Reyes-Gomez, I. Mora-Sero, G. Garcia-Belamonte, The Journal of Physical Chemistry Letters **8**(24), 6073 (2017).
[22] B. Hailegnaw, N. S. Sariciftci, M. C. Scharber, Physica Status Solidi A **217**(22), 2000291 (2020).
[23] X. Chen, Y. Shirai, M. Yanagida, K. Miyano, Journal of Physical Chemistry C **123**(7), 3968 (2019).
[24] Y. Yuan, J. Chae, Y. Shao, Q. Wang, Z. Xiao, A. Centrone, J. Huang, Advanced Energy Materials **5**(15), 1500615 (2015).

*Corresponding author: jiajooy@163.com